24

Cavity Enhanced Laser Cooling of Solids

Biao Zhong, Youhua Jia and Jianping Yin
State Key Laboratory of Precise Spectroscopy, Department of Physics,
East China Normal University, Shanghai 200062
P. R. China

1. Introduction

Since the successful realization of laser cooling of solids in 1995[1], the optical cooling techniques[2-5] have made fast development, and laser cooling experiments have obtained some important progress. However, how to improve the absorption of pump laser and enhance the temperature drops so as to realize the practical optical refrigeration, it has become a hot research point in applied physics. As early as 2002, the Heeg et. al proposed an extra- or intra-cavity enhancement scheme to improve the laser cooling effect of solids[2], and experimentally demonstrated their intra-cavity enhancement scheme in 2004, and found that there is no large temperature drops due to the experimental parameters were not optimized[3]. In 2003, Hoyt proposed a multiple-pass scheme to enhance the absorption of pump laser and did a series of experimental researches about the multiple-pass scheme[4]. As expected, a greater temperature drop was obtained. However, due to some limitation in the early work, it is difficulty to cool the sample to the cryogenics temperature, such as low absorption of cooling materials[5], the coating of the sample surfaces[3], the purity of the sample[6], the load from the ambient[1,7], etc. Therefore, people have done much work to improve the record of temperature drop. For example, to avoid the coating absorption deposited on the sample surface, they cut the sample with a Brewster angle along with the cavity axis[8], or improve the purity of cooling material[9-11], and so on. Mansoor. Seletskiy used the multi-pass scheme to do some meaningful experiments and obtain a milestone progress, that is, they cool a high pure Yb^{3+}-doped YLF to cryogenic temperature[12] in this year. To obtain an efficient absorption, another scheme was proposed to insert a Brewster-cut sample into a resonant cavity and make the cavity to be resonated with the pump laser, and then the maximum absorption of the pump laser can be achieved [2, 13-18]. Seletskiy demonstrated this scheme in the experiment[13]. However, this scheme depends on the power of the pump laser. Fortunately, the intra-cavity scheme proposed by Heeg can solve this problem in the case of low absorption[2]. He also suggested that inserting a cooling sample into the resonant cavity of a laser with a gain (so-called intra-cavity enhancement scheme) to realize the maximum absorption of the pump laser[2, 14, 19] and carried out it in the experiment[3].

Besides of enhancement laser cooling of bulk solids using resonant cavity, we propose another new scheme to optically cool some film materials (i.e., filmier solids) by using a high fineness planar waveguide, which is similar to the cavity enhanced cooling scheme. In our laser cooling scheme, the solid film as a high-index gap waveguide is separated from a prism by a low-index gap one, and an incident laser beam is resonantly coupled into a

waveguide mode through the gap, by frustrating total internal reflection. This will result in a large enhancement of the pump laser in the solid film and strengthen the effect of laser cooling.

In this chapter, some multi-pass, extra- and intra-cavity enhanced schemes for laser cooling of solids are reviewed and some experimental details of these schemes are discussed. In section 2, multi-pass laser pump scheme for laser cooling of solids are presented. In section 3, the basic principles of extra- and intra-cavity enhanced resonant absorption for laser cooling of solids are described, and the laser cooling effects between the multi-pass laser pump and cavity-enhancement schemes are compared. In section 4, some experimental results on laser cooling of solids using cavity-enhanced technologies and their recent progress are introduced in some detail and reviewed. Some main conclusions and outlook are summarized in the final section.

2. Multi-pass laser pump scheme for laser cooling of solids

In this section, the basic principles of the multi-pass laser pump scheme to increase absorption for the laser cooling of solids are briefly described, and the corresponding experimental results are introduced in some detail.

For the single pass pump geometry, the net power transferred to the sample for the laser radiation can be expressed as[8]

$$P_{net} = P_{abs}\eta_{cool} = [P_{in}(1-e^{-\alpha_{total}(\nu)L})][\frac{\alpha_b + (1-\widetilde{\eta_q})\alpha_r(\nu) - \alpha_r(\nu)\widetilde{\eta_q}\frac{h\nu_f - h\nu}{h\nu}}{\alpha_{total}(\nu)}]. \quad (2.1)$$

The negative P_{net} corresponds to laser cooling for solids. In Eq.(2.1), P_{in} is the incident laser power, P_{abs} is the absorption power of the sample, and η_{cool} is the cooling efficiency, α_b is the background absorption coefficient, which includes both the material's inherent absorption and the frequency-independent heat-generated absorption. α_r is the resonant absorption coefficient, $\alpha_{total}(\nu)$ is the total absorption, which includes a generalized background absorption (α_b) contributing to heating the sample, resonant absorption (α_r)and an effective absorption due to scattering losses (α_s), which describe the Fresnel reflections losses from the sample facets[20]. L is the physical path length of the laser beam in the sample. And ν and ν_f are the laser frequency and the mean fluorescent (which represents the mean fluorescent photon energy), respectively. $\widetilde{\eta_q}$ is the external quantum efficiency which represents the fraction of fluorescent emitting from the sample[21] and given by

$$\widetilde{\eta_q} \equiv \frac{\eta_e W_{rad}}{\eta_e W_{rad} + W_{nr}}. \quad (2.2)$$

The principle scheme of the multi-pass pump laser cooling for the cuboid solid sample[4] is shown in Fig 2.1. An incident pump laser beam goes into a solid sample by a hole on the first mirror, and is reflected back at a slightly sloped angle (or along the slightly deviating the incident direction) by the second concave mirror. Taking account of the first bracket term in Eq. 2.1, we can see that if we adopt the multiple pump passes geometry, it will be increased with the number of passes. If the P_{in} is the laser pump power before the first

mirror, then the absorbed power after multiply passing the sample with $\alpha_{total}(\nu)$ and the length L is expressed as[16]

$$\begin{aligned} P_{abs} &= P_{in}[1-\exp(-\alpha L)][1+R_2\exp(-\alpha L)+R_2R_1\exp(-2\alpha L)+ \\ &\quad +R_2{}^2R_1\exp(-3\alpha L)+R_2{}^2R_1{}^2\exp(-4\alpha L)+\ldots] \\ &\approx P_{in}[1-\exp(-\alpha L)][\frac{2-2(R_2R_1\exp(-2\alpha L))^n}{1-R_2R_1\exp(-2\alpha L)}] \\ &= P_{in}(1-e^{-\alpha_{total}(\nu)L})\frac{2-2S^N}{1-S} \end{aligned} \quad , \tag{2.3}$$

where N is number of passes, $S = R_2R_1\exp(-2\alpha L)$, R_1 and R_2 are the reflectance of the first and second mirrors, respectively.

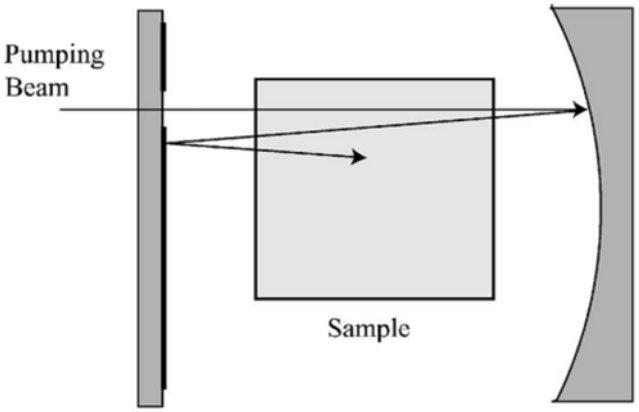

Fig. 2.1. Multiple-pass illustration scheme of cuboid sample laser cooling (figure from ref. [4])

To simplify equation 2.3, we can express the net power transferred to the sample as[3]

$$P_{net} = MP_{in}(1-e^{-\alpha_{total}(\nu)L})\eta_{cool}\,, \tag{2.4}$$

where $M = (2-2S^N)/(1-S)$, when η_{cool} is negative, P_{net} is also negative and represents the cooling power.

In recent years, Hoyt et al proposed and demonstrated three multiple-pass cooling schemes for solid sample and obtained some good results, which will be introduced as follows: The first is the Brewster sample multi-pass illustration scheme (see Fig.22). In this scheme, the solid sample is placed between the two mirrors, and the sample is cut as a cuboid geometric shape. It is clear that there are some disadvantages in this scheme, such as the Fresnel reflection losses from the sample facets, or the absorption pump laser contributing to heating due to the anti-reflection coating on the sample, etc. To avoid these disadvantages above mentioned, Hoyt et al used the Brewster-cutting geometry to reduce the Fresnel reflection losses from the sample facets by adjusting the polarization[4] of the incident laser beam.

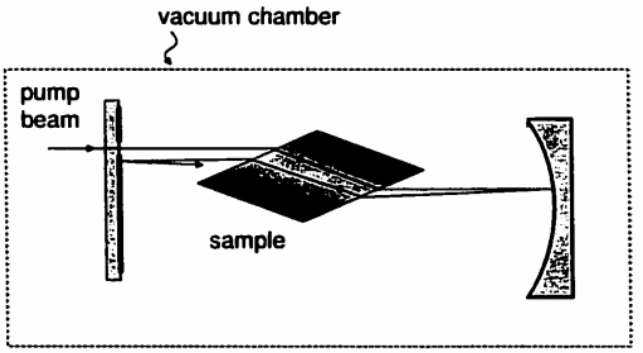

Fig. 2.2. Multi-pass illustration scheme of Brewster cut sample (figure from ref. [4])

The second scheme is the mirrored sample multiple-pass illumination (see Fig.2.3). In this scheme, the two mirrors are deposited directly on the samples, and the coating is exaggerated. There is a pore on one facet of the sample and the incident laser beam irradiates the sample by this hole, and the orientation of the pump beam deviates slightly the normal of the sample facet so as to multiply reflect the pump light in the sample back and forth. In this case, the absorption of the pump laser can be maximized.

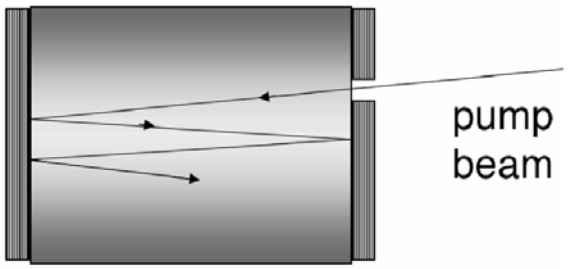

Fig. 2.3. Mirrored sample multiple-pass scheme (figure from ref. [4])

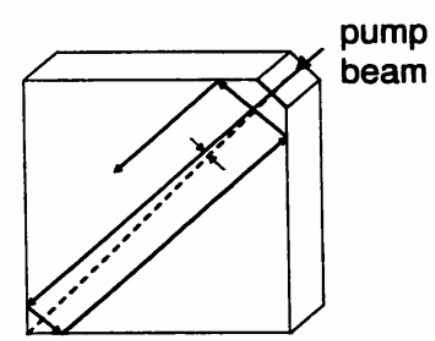

Fig. 2.4. Total internal reflection scheme of pump beam (figure from ref. [3])

The last scheme is the total internal reflection one of the pump laser beam, as shown in the Fig. 2.4. In this scheme, the total internal reflection is used to multiply reflect the pump beam in the sample and absorb the pump light as much as possible. For this, one vertex angle of the cubic sample at a diagonal is cut as a small square facet, and the pump beam goes into the sample from this square facet with a small departure, and then the pump laser beam can realize the total internal reflection in the sample, and then the pump beam can be almost absorbed.

On the other hand, the above three schemes have individual advantages. From the right term of Eq.2.5, we can see that if we want to maximize the net cooling power P_{net} deposited on the sample, we must maximize the factor M. Therefore in the second scheme when the mirrors are deposited directly on both sides of the sample, the factor M can be effectively maximized[3] because of a potential large number of passes (N). However, this will be detrimental for obtaining a potential large α_b due to the mirror absorption of the pump laser and resulting in a heating. This can be avoided in the first scheme because the mirrors are placed at the outsides of the cooling sample, and the effective background absorption will leave the material alone. Unfortunately, M is no longer maxima due to the finite scattering losses (e.g. Fresnel reflections), and there is also the difficulty of the maximizing N, but if adopting the Brewster-cut sample, the facet reflections are negligible and the factor M can be increased.

Hoyt et al made a cylindrical 1 wt% Tm^{3+}: ZBLANP sample with a radius of ~3mm and did some experimental researches for the above scheme[4, 8]. In this experiment, the highly-reflecting dielectric mirrors (Cascade optical) are deposited directly on both sides of the sample, and a small entrance aperture for the pump beam is made in one of the mirrors. After coupling the pump laser beam into the sample, unfortunately, the heating effect was observed at all pump wavelengths instead of cooling in the expected wavelength. The experimental results in Fig. 2.5 tell us that the heating magnitude varies with the pump wavelength[22]. From Fig. 2.6, it is obvious that there is the water absorption in the mirrors, and this water absorption in the mirrors are contained in the effective total absorption[22] (i.e. added to α_b =0.0002 cm^{-1}) distributed across the sample length in the mathematics.

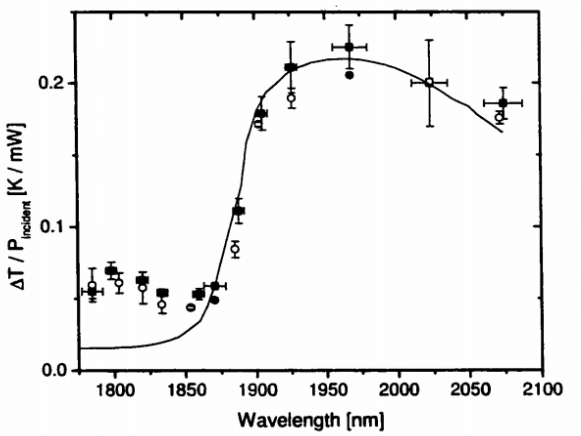

Fig. 2.5. Mirrored sample heating with qualitative fit using water absorption (figure from ref. [4])

If using Eq. 2.6[8] with an additional absorption due to water in the mirrors to fit the experimental data in Fig 2.5, we can obtain the expression of the temperature drop of the sample as follows

$$\frac{\Delta T}{P_{in}} \approx \kappa[\alpha_b + \alpha_r(\nu)(1-\widetilde{\eta}_q) - \alpha_r(\nu)\widetilde{\eta}_q \frac{\lambda - \lambda_f}{\lambda_f}] \tag{2.6}$$

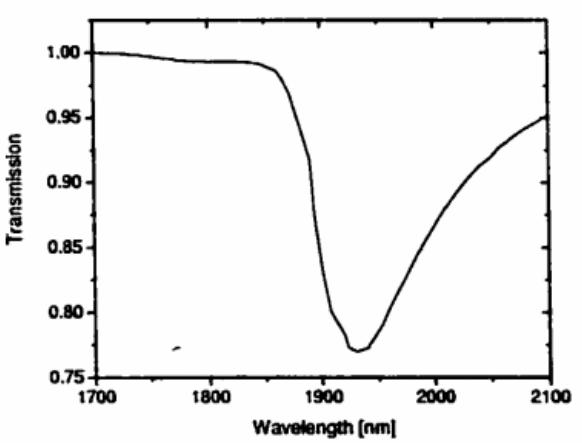

Fig. 2.6. Transmission spectrum of the cooling sample with a length of 20 μ m (figure from ref. [4])

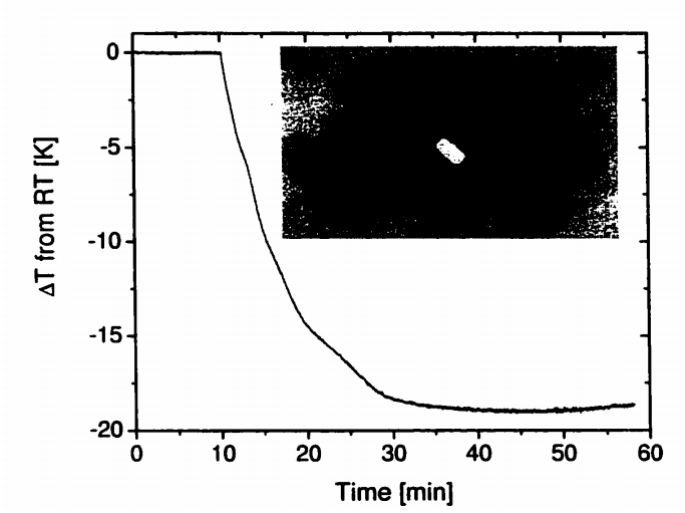

Fig. 2.7. The temperature drops from the room temperature. The bright areas correspond to cooling and the dark to heating (figure from ref. [4])

The solid line in Fig. 2.5 represents the quantitative fitting. From Fig.2.5 we can see that the change of the sample temperature is dependent on the wavelength of the pump laser. Fig. 2.7 shows the cooling results of the multiple-pass pumped cuboid sample in a non-resonant cavity configuration. The pump power is about 3.5W at a wavelength of 1.9μm. We can see from Fig. 2.7 that after the sample is illuminated by the pump laser, the sample temperature starts to be dropped at about 10min, and the sample was cooled to 19 K below the room temperature at the 30min and the sample temperature is no longer changed after ~ 30min. This shows that the net cooling is obvious because the heating from the mirrors that directly deposited on the sample is eliminated, however, the parameters *M* is not optimized because the pump beam undergoes 4% Fresnel losses at one facet of the sample at each pass[20].
To avoid the Fresnel losses, Hoyt et al. used the Brewster-cut sample in the non-resonant cavity to improve experimental results, and the corresponding experimental setup and results are shown in Fig. 2.8 and table 2.1. Here the OPO beam is the pump source with a power of 4.35W and 4.5W, which are coupled into the first facet of the two samples, respectively. In the two experiments, the cavity length is about 11cm and the second concave mirrors has a radius of 20 cm, and the change of the sample temperature was measured by recording the phase change in a calibrated Mach-Zehnder interferometer.

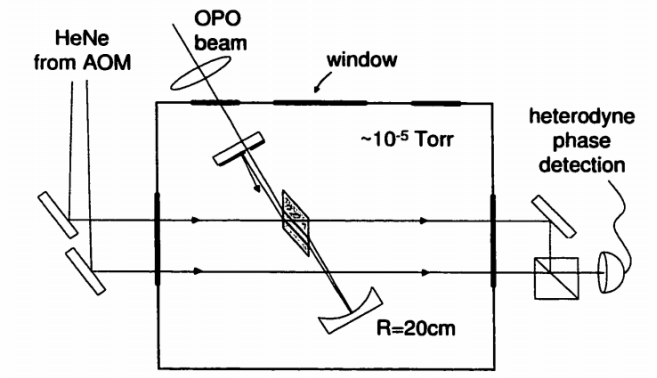

Fig. 2.8. Laser cooling setup using Brewster-cut sample in non-resonant cavity (figure from ref. [4])

Sample	ΔT from RT [K]	P_{abs} [W]	P_{cool} [mW]	τ_{fit} [s]	τ_{calc}
Tm C	-19	2.23	73	13.8	12
Tm D	-24	1.22	40	9	7.8

Table 2.1. The cooling results of Brewster-cut sample (table from ref. [4])

In the table 2.1, τ_{fit} is the fitted time constant, and τ_{calc} is the theoretical time constant from the equation[4]

$$\tau = \frac{c_m \rho V_s (1+\chi)}{4\varepsilon_s \sigma A_s T_C^3}, \tag{2.7}$$

where c_m is the heat capacity per volume, ρ is the sample density, V_s is the sample volume, T_c is the chamber temperature, A_s is the sample surface area, and σ is the Stefan-Boltzmann constant. In addition, the χ in Eq. 2.7 is defined as

$$\chi \equiv (\varepsilon_s A_s / \varepsilon_c A_c)(1-\varepsilon_c), \tag{2.8}$$

where $\varepsilon_{s,c}$ is the emissivity of the sample and chamber. Assuming the unity emissivity for sample and chamber, we can find from table 2.1 that τ_{fit} are 13.8min and 12min for the two samples, while τ_{calc} are 12min and 7.8min, respectively. So the difference between τ_{fit} and τ_{calc} are approximately 15%, but if presuming the sample emissivity is 0.9, the difference between τ_{fit} and τ_{calc} is reduced to about 5% in the both cases.

Hoyt et al studied the dependences of laser cooling power on the number of passes *N* for three different multi-pass schemes: cuboid sample with Fresnel losses in the non-resonant cavity, Brewster-cut sample with the same condition as cuboid sample, and a similar sample with the mirrors deposited directly on its facets, and the experimental results are shown in Fig. 2.9.

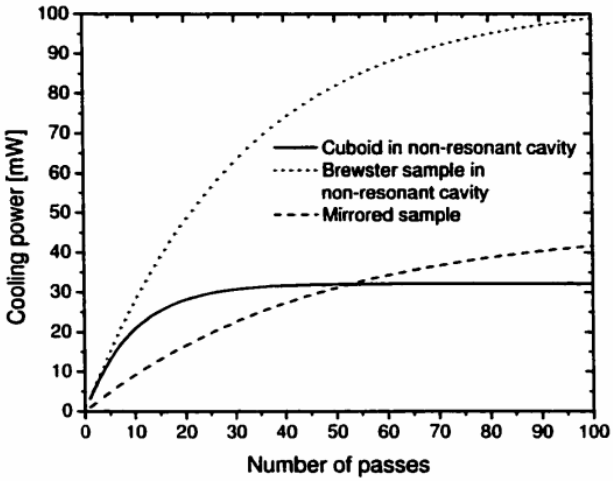

Fig. 2.9. Cooling power modeling for samples with cuboid and Brewster respectively, placed in a non-resonant cavity and a sample with mirrors deposited directly on its facets. (Figure from ref. [4])

In Fig. 2.9, the solid line represents the cuboid sample in non-resonant cavity according to Eq.2.5, and setting the parameters as follows: α_b =0.0002 cm^{-1}, α_r =0.025 cm^{-1}, $\widetilde{\eta_q}$ =0.99 and the sample length is 0.84 cm, the scattering losses α_s and Fresnel loss about 4% at each facet per pass are included in the total effective absorptivity α_b. The power of pump beam is 1.5W at a wavelength of 1.9μm, and the mean fluorescent wavelength is 1.803μm. The doted line shows the cooling power with the same condition as cuboid sample except without the Fresnel losses due to Brewster-cut surface. Taking into account the little loss on the Brewster cut facets, so setting that a loss values is 0.5% per pass in each facets. The dashed line is also the same calculation other than the mirrors deposited directly on the surface of the sample. Then in the case of α_s =0, the absorption in the mirrors can be added into the background

absorption distributed across the sample length[4], so we can set α_b =0.0002 cm^{-1}. The parameters for calculating the cooling power for the mirrors attached directly on the two sides of the samples are arbitrary because it lies on the background absorption in the mirrors[4]. So it is the most important for cooling power that reducing the mirror's absorption. If the reflectance of the mirror deposited directly on the sample is 99.95%, then the remaining 0.05% power was absorbed by the mirrors. As the above discussed, we add this absorption into the background absorption distributed across the sample length. So each mirror has an optical density (OD) of $(\alpha L)_{mirror}$ =0.0005.

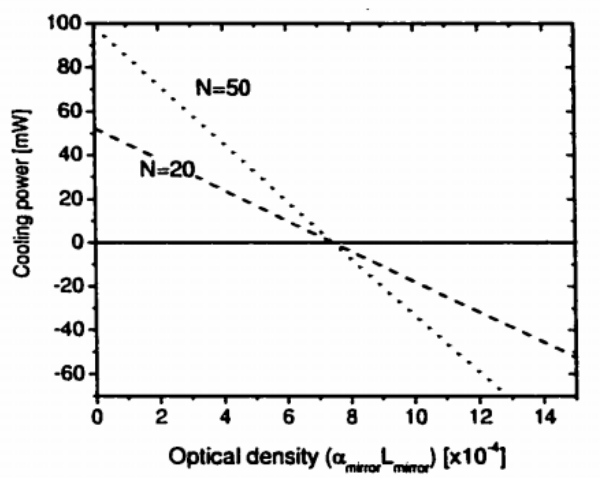

Fig. 2.10. The relationship between the cooling power and optical density (OD) in the scheme of mirror deposited directly on the samples. (Figure from ref. [4])

Fig. 2.10 describes the relationship between the optical density (OD) and the cooling power for N=50 and 20, respectively. From Fig. 2.10, we can find that the OD must less than the certain value otherwise the cooling power will be become a negative value, which can also be seen from Fig. 2.10. If the value of the OD is larger than 0.00078, there will be no cooling was observed.

In 2010, D. Seletskiy's group prepared the home-prepared high-purity 5% ytterbium-doped YLF crystal and cooled it down to the cryogenic temperatures, and the absorption, emission and cooling efficiency spectra of the 5% doped Yb^{3+} YLF crystal is shown in Fig.2.11.

In Fig. 2.11, figure (a) represents the absorption and emission spectra, and (b) describes the cooling efficiency. Fitting the experimental cooling efficiency using Eq. 2.9 [23], we can obtain $\eta_{ext} = 0.995$ and $\alpha_b = 4.2 \times 10^{-4} cm^{-1}$.

$$\eta_c(\nu, T) = \eta_{ext}[\frac{1}{1+\alpha_b / \alpha(\nu, T)}]\frac{\tilde{\nu}_f(T)}{\nu} - 1, \tag{2.9}$$

where η_{ext} is the external quantum efficiency, α_b is the background absorption, $\alpha(\nu, T)$ is the resonant absorption coefficient of the active ion, and $\tilde{\nu}_f$ is the frequency of the escaped mean luminescent photon, including the reabsorption effect of the emitted fluorescent photon.

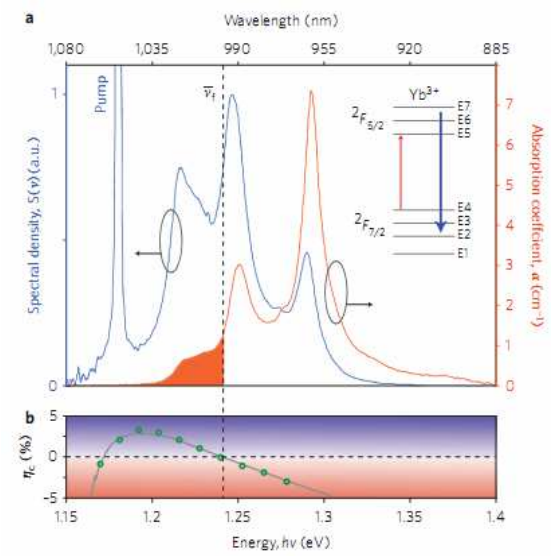

Fig. 2.11. Absorption, emission and cooling efficiency spectra of the 5% doped Yb^{3+} YLF crystal. The red and blue lines are the absorption and emission spectra respectively for a pump laser with λ=1055nm and polarization along the c-axis. The shade of the red line is the cooling tail. Inset: $^2F_{5/2}$ and $^2F_{7/2}$ levels in the crystal position containing seven stark manifolds. Figure b, cooling efficiency curve, the open circles is the experimental data and the line is the mode fitting one. (Figure from ref. [12])

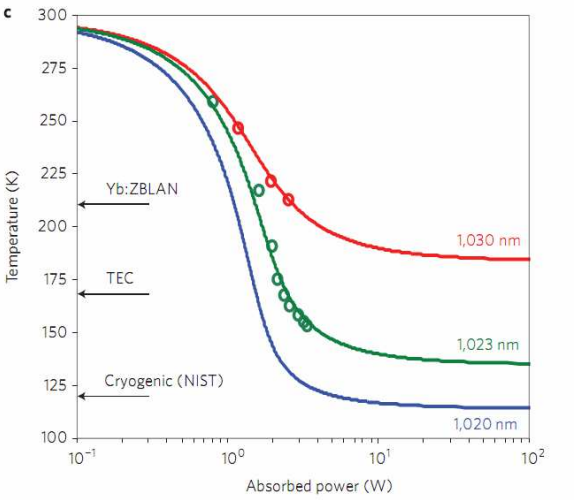

Fig. 2.12. Dependences of the sample cooling temperature on the absorbed power for different pump laser wavelength. The open circles are the experimental data and the solid lines are the mode fitting curves from Eq. 2.10. The blue line indicates the sample used in the experiment can achieve the minimum temperature. (Figure from ref. [23])

Fig. 2.12 shows the dependences of the cooling temperature of Yb: YLF sample for the pump wavelength at $\lambda = 1020$nm, 1023nm and 1030nm, respectively. According to the experimental data in Fig. 2.12 and the Stefan-Boltzmann law associated with the measured $\eta_{abs}(\nu, T)$ and η_{ext} , the dependence of the sample cooling temperature on the absorbed power can be modeled[23] as

$$\eta_c(\nu, T) p_{abs}(\nu, T) = \kappa(T_C^4 - T^4) , \tag{2.10}$$

where T_c is the chamber temperature, and κ is the radiation load constant depending on the geometry and joint thermal emissivities of chamber and sample.
In Fig. 2.12, the red, green and blue lines represent the cases of the pump laser wavelength of 1030nm, 1023nm and 1020nm, respectively. The above arrow indicates the previous cooling record in ytterbium-doped ZBLAN glass, the middle arrow shows the standard thermoelectric coolers (TEC) and the below arrow indicates NIST-defined cryogenic temperature. In this experiment at the maximum available absorbed power of 3.5W at 1023nm, the sample is cooled to $155K \pm 1K$ absolute temperature, and the heating is lifted up to 90mW.

3. Resonant cavity-enhancement schemes for laser cooling of solids

In this section, we review the basic principles and theoretical researches of laser cooling of solid in resonant extra- or intra-cavity, and compare the laser cooling results in the above schemes. Furthermore, we compare the cavity-enhancement schemes with the multi-pass enhancement absorption one.

3.1 Extra-cavity enhancements for laser cooling of solids

Fig. 3.1 shows the scheme of the extra-cavity enhancement for laser cooling of solids. As shown in Fig. 3.1, the two mirrors with a reflectivity R_1 and R_2 are composed of a resonant extra-cavity, and the cooling medium with an absorption coefficient α is placed between the mirrors. According to the Beer Law, the loss of the pump beam is proportional to $e^{-\alpha d}$ in each pass, and in the same time the other losses including the reflection on the surface of sample and its scattering is defined as x, the pump laser with an intensity of I_0 is coupled into the cavity, and pump/illuminate the sample with a length of L and a lower absorption. The pump beam is reflected on the two cavity mirrors back and forth. If the cavity is resonant with the pump laser, consequently, the beam intensity in the cavity will be resonantly enhanced, and the absorption of cooling sample will be also enhanced.

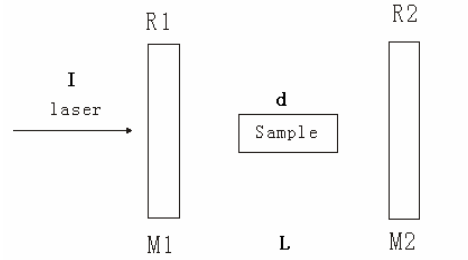

Fig. 3.1. The principle scheme of extra-cavity enhancement for laser cooling of solids (Figure from ref. [16])

Here we assume that the amplitude of the pump laser is E in the cavity and the corresponding intensity is I, while the amplitude of the incident laser beam before the first mirror R_1 is E_0 and the corresponding intensity is I_0, and then the amplitude of the laser after each time reflection from R_1 and R_2 are given by

$$E^2 \times (1 - R_1) = {E_0}^2, \tag{3.1}$$

$$E_1 = E_0 r_1 r_2 \exp(ik \times 2L), \tag{3.2}$$

$$E_2 = E_1 r_1 r_2 \exp(ik \times 2L), \tag{3.3}$$

$$E_n = E_{n-1} r_1 r_2 \exp(ik \times 2L), \tag{3.4}$$

where $r_{1,2}$ are the amplitudes of the reflectivity of the first and second mirrors respectively, and then the total amplitude of the pump beam forward to the right can be expressed as

$$E_a = E_0 \sum_{n=1}^{\infty} (r_1 r_2)^{2(n-1)} \exp[ik \times 2(n-1)L] = \frac{E_0}{1 - r_1 r_2 \exp(ik \times 2L)}, \tag{3.5}$$

and the corresponding intensity is

$$I_a = E_a \times {E_a}^* = \frac{I_0}{(1 - r_1 r_2 e^{i\delta})(1 - r_1 r_2 e^{-i\delta})} = \frac{I_0}{1 + (r_1 r_2)^2 - 2 r_1 r_2 \cos\delta}, \tag{3.6}$$

where $\delta = 2kL$. When the laser is resonant with the cavity, we have

$$\cos\delta = 1 \quad , \quad I_a = \frac{I_0}{1 + (r_1 r_2)^2 - 2 r_1 r_2}. \tag{3.7}$$

Assuming the axis of optical cavity is the x axis, the total amplitude of pump laser in the cavity is given by

$$E = (E_a e^{jkx} + E_{a'} e^{-jkx}) e^{-jwt} = 2 E_a j \sin kx e^{-jwt}, \tag{3.8}$$

and the corresponding intensity of the pump beam is

$$I = \tilde{E} \times \tilde{E}^* = I_a (1 - \cos 2kx). \tag{3.9}$$

Then the mean intensity of the pump beam can be written as[16]

$$\bar{I} = \frac{I_0}{1 + [r_1 r_2 (1-x) e^{-\alpha l}]^2 - 2 r_1 r_2 (1-x) e^{-\alpha l}}. \tag{3.10}$$

In final, the mean enhancement factor is defined as a ratio of the mean intensity of the pump beam in the cavity to the initial intensity of the incident laser beam and given by [16]

$$E_{cav} = \frac{p_{circl}}{P_{in}} = \frac{\bar{I}}{I} = \frac{(1 - {r_1}^2)}{1 + [r_1 r_2 (1-x) e^{-\alpha l}]^2 - 2 r_1 r_2 (1-x) e^{-\alpha l}}. \tag{3.11}$$

We take the ZBLAN for an example and set x= 0.05, l=3mm, and α =0.09cm^{-1}, and study the dependence of the enhancement factor E_{cav} of the pump laser in the cavity on both the amplitude r_1 of the reflectivity of the first mirror R_1, and the sample length, and the results are shown in Fig.3.2.

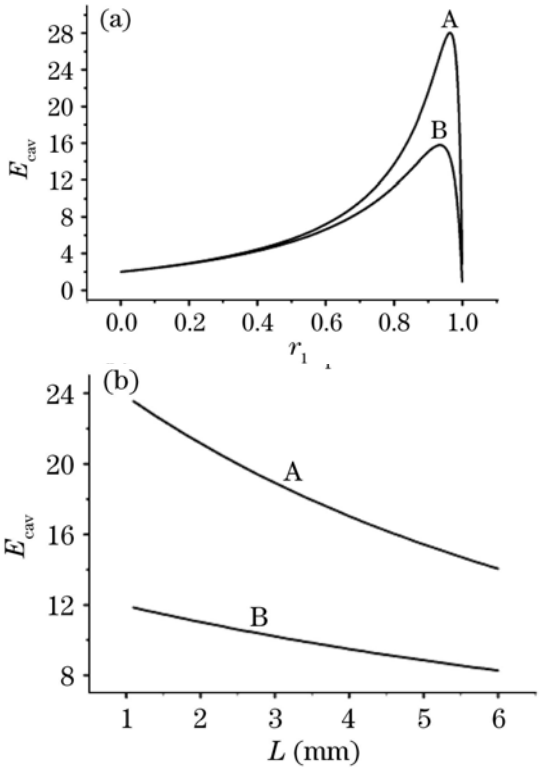

Fig. 3.2. (a) The relationship between the enhancement factor E_{cav} of the pump laser in the cavity and the amplitude of the reflectivity of the first mirror. (b) The relationship between the enhancement factor E_{cav} and the sample length L. (Figure from ref. [16])

In Fig. 3.2 (a), the curve A is the case of the sample surface with an AR coating, which can be used to reduce the losses of reflection on the sample surfaces so as to enhance the intensity of the pump beam in the cavity. The curve B is the case of the sample's surface without an AR coating. It can be seen from the curves A and B that when the reflection loss from the sample surfaces is reduced from the 0.04 to the 0.01, the enhancement factor of the pump laser in the cavity is enhanced from the 15 to 28. From Fig. 3.2(b), we can see that with the increasing of the sample length, the enhancement factor will be reduced. This is because the absorption of sample will follow the Beer Law. This shows that by reducing the sample length, one can obtain higher enhancement factor of the pump beam in the cavity, but it also reduce the cooling power. So it is must be taken into account an optimal sample length and a cooling power as high as possible.

Then we use the two energy level system to analyze the Yb^{3+} level transition between $^2F_{7/2} \rightarrow {}^2F_{5/2}$, and obtain an expression of the cooling power in the Extra-cavity enhancement scheme [24] as follows

$$P_{cool} = \frac{N\sigma_{abs} L\alpha_{eff} I_s (\lambda / \lambda_{F^*} - 1)}{1 + \sigma_{se} / \sigma_{abs} + \alpha_{eff} I_s / P}, \tag{3.12}$$

where α_{eff} is the effective irradiation area of the sample, P is the power of pump laser, and I_s is the characteristic wavelength-dependent saturation intensity[19], which is defined as

$$I_s = hc\gamma_{rad} / \lambda\sigma_{abs}, \tag{3.13}$$

where σ_{abs} and σ_{se} are the absorption and stimulated emission cross-sections respectively, λ is the wavelength of the pump laser, and λ_{F^*} is the effective mean fluorescent wavelength[7], which can be defined as

$$\lambda_{F^*} = (\frac{1}{\lambda_F} - \frac{\kappa}{hc\gamma_{rad}})^{-1}. \tag{3.12}$$

According to Eq 3.12, we study the dynamic process of the cooling temperature for different pump power, and the results are shown in Fig.3.3. In our calculation, the used parameters come from Ref. [7].

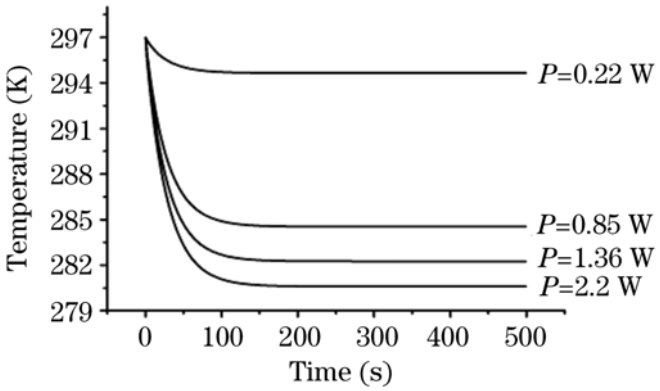

Fig. 3.3. Temperature drop with different pump laser power (Figure from ref. [16])

From Fig.3.3, we can find that with the increase of the pump power from 0.22W to 2.2W, the temperature of the cooling sample will be reduced from 294.6K to 280.5K. This shows that the extra-cavity enhanced laser cooling for solid is also very effective.

In 2006, D. Seletskiy et al proposed another method to describe the extra-cavity resonant enhancement for optical refrigerator. They assumed that the reflectivity R_2 of the second mirror of the cavity is approximately equal to 1, the absorption coefficient A of the cavity is defined as[13]

$$A = 1 - (T + R), \tag{3.13}$$

or

$$A = \frac{1 - \Delta}{1 + F \sin^2 \delta}, \tag{3.14}$$

where

$$\Delta = \frac{(\sqrt{R_{ic}} - e^{-\alpha l})^2}{(1 - e^{-\alpha l}\sqrt{R_{ic}})^2}, \tag{3.15}$$

$$F = \frac{4e^{-\alpha l}\sqrt{R_{ic}}}{(1 - e^{-\alpha l}\sqrt{R_{ic}})^2}, \tag{3.16}$$

and R_{ic} is the input coupling reflectivity and $\delta = kl$, k is the wave vector inside the absorbing material here assuming that the material fills up the whole cavity, and l is the length of cooling material, and α is the absorption coefficient. From Eq. 3.14, it is clear that A can be achieve to be unity when Δ and $\sin\delta$ are set to be zero, i.e., when $R_{ic} = e^{-2\alpha l}$ and $\delta = m\pi$.
From the above two methods, we find that when the reflectivity R_1 of the in-couple mirror is about 95% in the case of setting the same sample absorption, the intensity of the pump beam in the cavity and the absorption of the pump laser can achieve the maximum value.
Similar to the extra-cavity resonant enhancement laser cooling scheme for solids, we proposed a resonant waveguide structure (see Fig.3.4) to effectively cool solid sample, which will enhance the intensity of an evanescent wave by more than two orders of magnitude in the doped Yb^{3+} YAG film with a refractive index n_3. The waveguide structure for this scheme is consisted of a prism and two waveguides, which form three layer films with different refraction index n_1, n_2 and n_3 from the bottom to up, here $n_2 < n_1 < n_3$. The enhancement principle of this resonant waveguide scheme is similar to a Fabry-Perot cavity with a high finenss[25]. On the doped Yb^{3+}YAG film-vacuum interface, the light is totally reflected, corresponds to the second mirror of the cavity with a reflection coefficient of 1.0. We thus have a Fabry-Perot cavity with a high fineness: for given values of incident light parameters (e.g. the wavelength), the light field amplitude inside the waveguide will experience a strong resonant enhancement.

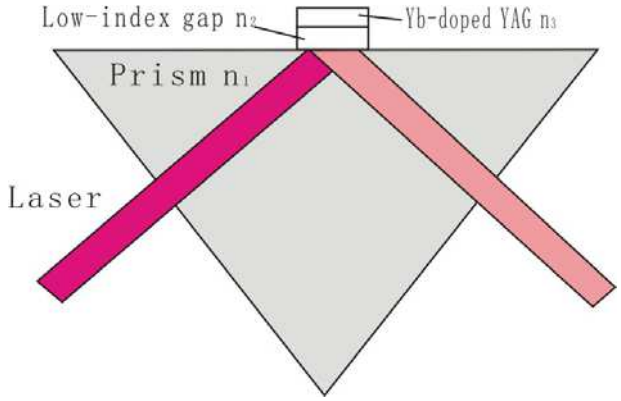

Fig. 3.4. Scheme of resonant waveguide enhancement for laser cooling of solids

We calculate the enhancement factor of the pump laser in the resonant waveguide structure for the different thickness of doped Yb^{3+}YAG film, and the results are shown in Fig.3.5.

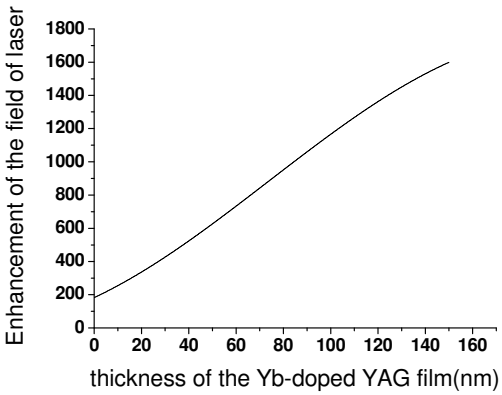

Fig. 3.5. Dependence of enhancement factor on the thickness of Yb-doped YAG film

It is clear from Fig.3.5 that with the increase of the thickness of Yb-doped YAG film, the enhancement factor of the intensity inside Yb-doped YAG film will be greatly increased. In particular, when the thickness of Yb-doped YAG film is increased from 10nm to 160nm, the enhancement factor will be increased from about 200 to 1600 times. This shows that our proposed resonant waveguide enhancement scheme can be used to efficiently cool the solid film material.

3.2 Intra -cavity enhancements for laser cooling of solids

The extra-cavity resonant enhancement technology is useful to laser cooling of solids due to the greatly-increased pump laser intensity. However, because the partial transparence of in-couple mirror M_1 ($R_1 < 1$) confines the pump power coupled into the cavity (that is, there is a coupling loss from M_1), the enhancement of pump-beam intensity and the cooling effect of the sample is limited. However, if placing a cooling sample into a resonant cavity of with a gain, we can obtain a greater pump-laser power for laser cooling of solids. This is so-called the intra-cavity cooling scheme, which is shown in Fig. 3.6. In this scheme, the cooled sample is inserted in the resonant cavity of laser with a gain, and the two mirrors (M_1 and M_2) with a reflectivity R_1 and R_2 are the two resonant-cavity mirrors of laser with a gain coefficient g_0 . In this case, the two main losses, the absorption loss of sample and the reflection loss of sample surfaces, are added into the original loss δ_0 of the used laser, which forms a total loss δ for the laser. As long as $g_0 \geq \delta$, the used laser can be still satisfied its resonant condition and form a stable laser oscillation. It is clear that the laser intensity in such a laser cavity is far higher than one in a conventional laser because the reflectivity R (= $R_1 = R_2$) of the mirrors in our proposed intra-cavity cooling scheme can be higher than one R_2 of the output mirror M_2 in a conventional laser. So the intensity of the pump laser in intra - cavity resonant enhancement scheme will be greatly amplified, and an efficient laser cooling for solids will be obtained.

Fig. 3.6. Intra-cavity cooling scheme for solids (figure from ref. [14])

It is well known that the output power of a conventional laser system is given by [26]

$$P_{out} = \frac{1}{2} A I_s T \left(\frac{2g_0}{T + \delta_0} - 1 \right), \tag{3.17}$$

where I_s is the saturation parameter of laser system, A is the average effective cross section, g_0 is the gain coefficient of laser, δ_s is the loss on the surface of sample, δ_0 is the original loss in laser cavity. When the cooling sample is placed in a resonant cavity of laser, the circular power in the cavity is given by [26]

$$P_{circ} = \frac{1}{2} A I_s \left(\frac{2g_0}{T + \delta_0 + \delta_S + 2\alpha d} - 1 \right), \tag{3.18}$$

and then the enhancement factor can be expressed as[14]

$$M = \frac{P_{circ}}{P_{out}} = \frac{\dfrac{2g_0}{T + \delta_0 + \delta_S + 2\alpha d} - 1}{T\left(\dfrac{2g_0}{T + \delta_0} - 1 \right)}. \tag{3.19}$$

In the low gain case, assuming $g_0 = 0.084$, $\delta_0 = 0.076$, $\delta_S = 0.004$, and the sample length is d=3cm and $\alpha = 0.09 cm^{-1}$, for Yb^{3+}-doped material. When d=2mm, 3mm, 4mm, according to Eq. 3.19, we study the dependence of the enhancement factor M on the transmittance T of the mirror M_2, and the results are shown in Fig. 3.7.

From Fig.3.7, we can see that with increasing of the sample length, the enhancement factor will be reduced because the longer the sample length is, the more the sample absorption of the pump laser is according to Beer Law. However, for a given sample length, the enhancement of the pump beam intensity will be reduced with the increase of the transmissivity T of the output mirror M_2 due to the increase of the output loss from the mirror M_2. The cooling power of the perfect sample placed in the intra-cavity can be described as[1]

$$P_{cool} = P_{abs}\eta = P_{abs}\frac{\lambda - \lambda_f}{\lambda}, \tag{3.20}$$

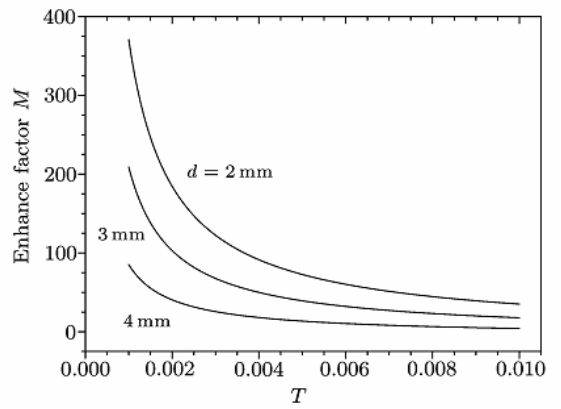

Fig. 3.7. Enhancement factor as a function of transmittance T of the mirror M_2 for different sample length (Figure from ref. [14])

where P_{abs} is the absorption power of the sample, η is the quantum efficiency that will be slightly reduced during the temperature drop of the sample, simultaneously the mean fluorescent wavelength will be red shift[26], and we have

$$P_{abs} = P_{circ} \times (e^{\alpha d} - 1) . \tag{3.21}$$

Substituting Eq.3.21 into Eq.3.20, and making the assuming that αd is small, Eq. 3.21 can be approximately as[14]

$$P_{abs} = \frac{1}{2} \alpha d A I_s (\frac{2g_0}{T + \delta_0 + \delta_S + 2\alpha d} - 1) . \tag{3.22}$$

From Eq.3.22, it is obvious that for the some sample the absorption power of the sample depends on both the sample length and the transmissivity of the output mirror M_2. It is clear in physics that the longer the sample length is, the more the absorption power of the sample is, and then the increasing cavity loss will result in the reduction of the laser oscillating intensity in the cavity. So there must be the optimal length, which can lead to the maximum P_{abs} .

By solving the steady-state solution of Eq.(3.22), that is, by solving $\frac{d(P_{abs})}{d(\alpha d)} = 0$, we can obtain the relationship between the optimal sample length d_{opt} and the transmissivity T of the output mirror as follows[14]

$$\alpha d_{opt} = \frac{1}{2} \left[\sqrt{2g_0 (T + \delta_0 + \delta_S)} - (T + \delta_0 + \delta_S) \right] , \tag{3.23}$$

and the corresponding maximum absorption power is[14]

$$P_{abs,\max} = \frac{1}{4} A I_s (\sqrt{2g_0} - \sqrt{T + \delta_0 + \delta_S})^2 . \tag{3.24}$$

Fig. 3.8 shows the dependence of the optimal sample length on the transmittance T of the output cavity mirror M_2.

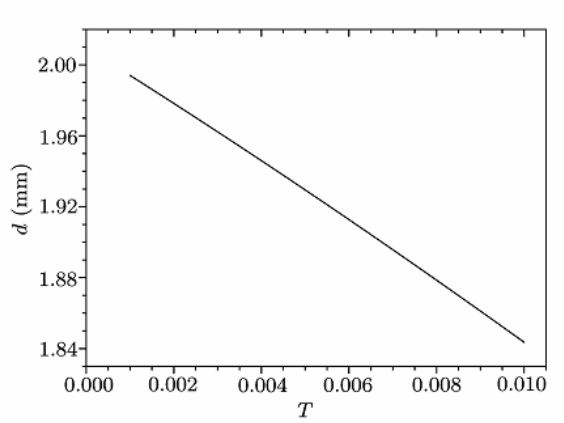

Fig. 3.8. Optimal sample length as a function of transmittance T of the output mirror M_2 (Figure from ref. [14])

It is clear from Fig.3.8 that the optional sample length will be nearly linearly reduced with increasing the transmittance T of the output mirror M_2. In particular, the sample length does not exceed 2mm in order to obtain a higher enhancement factor and better cooling effect.

3.3 Comparison between multi-passes pump and cavity-enhancement schemes

The enhancement of three schemes, multi-passes, extra-cavity and intra-cavity, are analyzed in the section 2, sub-section 3.1 and 3.2 respectively, and these schemes have their different advantages. In this section, we will compare make the comparison between the multi-pass pump scheme and two cavity-enhancement ones, and hope that one can learn some guiding sense.

Firstly, we compare the multi-passes pump scheme with the extra-cavity enhancement one. According to Eq. 2.3, when the reflection times N of the pump beam approach an infinite value, we can obtain the maximum absorption power as follows [14]

$$P_{abs} = P_{in}[1-\exp(-\alpha L)][\frac{2}{1-R_2R_1\exp(-2\alpha L)}] = 9.7\times P_{in}[1-\exp(-\alpha L)], \tag{3.25}$$

where assuming $R_2 = R_1$ =99.9%. However, in the extra-cavity enhancement scheme, the absorption power can be described as

$$\mathrm{P}_{abs} = P_{circ}[1-\exp(-\alpha L)], \tag{3.26}$$

where $P_{circ} = E_{cav}P_{in}$, according to Eq.3.26 and setting the same parameters, we can obtain $P_{circ} = 13.8P_{in}$. It is clear that the enhancement factor in the extra-cavity resonant (absorption) scheme is larger than that in the multi-passes one. By comparing the temperature drop in the above two schemes, one can easily observe the advantages of the cavity-enhancement. The temperature drop of the cooling sample can be given by [6]

$$\frac{C_m \rho_m \pi D^2}{4} \frac{d(T_S - T_r)}{dt} = P_{load}(T_S) - P_{cool}(T_S), \tag{3.27}$$

and $$P_{load} = A\int \varepsilon_\nu \pi \frac{\partial B_\nu(T)}{\partial T} \Delta T d\nu = 4\pi D \varepsilon \sigma_B T_r^3 \Delta T = \pi D \varepsilon \sigma_B (T_r^4 - T_S^4), \tag{3.28}$$

wgere S is the cross section of the sample, P_{load} is the radiative and conductive load, C_m is the specific heat, ρ_m is the mass density, T_S and T_r are the sample and room temperatures, respectively. Fig. 3.9 is the results of the temperature drop of the multi-passes pump and extra-cavity enhancement schemes.

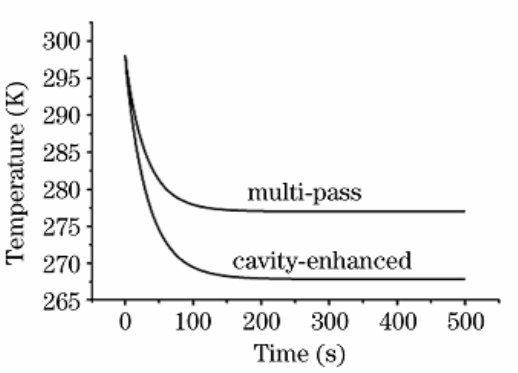

Fig. 3.9. the temperature drop comparison between the multi-pass pump and the extra-cavity enhancement schemes (Figure from ref. [14])

From Fig. 3.9, we can find that under the same parameters, the limit of temperature drop in the multi-pass pump scheme is smaller than that in the extra-cavity enhancement one. That is, the cooling effect of the extra-cavity enhancement scheme is better than one of the multi-pass pump one.

Usually, in the resonant extra-cavity enhancement scheme, the absorption power of the sample for the pump can be easily calculated by the multi-absorption. However, in the intra-cavity enhancement scheme, before calculating the absorption power of of the sample for the pump laser, we first have to calculate the laser power in the cavity.

In order to compare the intra-cavity enhancement scheme with the extra-cavity one, we define the input power of the extra-cavity by the gain-saturation formula[26]

$$P_{in} = \frac{1}{2} A I_s T \left(\frac{g_0}{T + \delta_0} - 1\right), \tag{3.29}$$

where T is the transmittance of the couple mirror M_1, I_s is the system saturation parameter, and g_0 is the gain of laser gain medium.

Once the pump beam passes the sample, the absorption power of the sample for the pump laser can be expressed as[2, 19]

$$P_{abs,s}^{ext} = (1 - e^{-\alpha L})(1 - R_s) P_{in} = \frac{1}{2}(1 - T_s)(1 - R_s) A I_s T \left(\frac{g_0}{T + \delta_0} - 1\right). \tag{3.30}$$

After the pump beam Nth passes through the sample, the total effective absorption power of the sample is given by [2, 19]

$$P_{abs}^{ext} = \frac{1}{2}(1-e^{-\alpha L})(1-R_s)AI_sT(\frac{g_0}{T+\delta_0}-1)\sum_{n=1}^{N}(\theta T_S)^{n-1} \tag{3.31}$$

$$= \frac{1}{2}(1-e^{-\alpha L})(1-R_s)AI_sT(\frac{g_0}{T+\delta_0}-1)\frac{1-(\theta T_S)^N}{1-\theta T_S}. \tag{3.32}$$

By optimizing the output coupler ($d P_{in} / dT=0$) for maximum P_{in}, we have

$$T_{opt} = \sqrt{g_0\delta_0} - \delta_0 . \tag{3.33}$$

So the maximum of P_{abs}^{ext} can be obtained by [2, 19]

$$P_{abs,opt}^{ext} = \frac{1}{2}(1-e^{-\alpha L})(1-R_s)AI_sT(\sqrt{g_0}-\delta_0)^2\frac{1-(\theta T_S)^N}{1-\theta T_S}. \tag{3.34}$$

For the sake of convenience, Eq. 3.34 and 3.21 are written in dimensionless, respectively [2, 19]

$$P_{abs,opt}^{ext} = (1-e^{-\alpha L})(1-R_s)(\sqrt{g_0}-\delta_0)^2\frac{1-(\theta T_S)^N}{1-\theta T_S}, \tag{3.35}$$

and

$$P_{abs} = \alpha d(\frac{2g_0}{T+\delta_0+\delta_S+2\alpha d}-1). \tag{3.36}$$

Under the low gain conditions, and according to Ref [3], we have g_0 =0.089 and δ_0 =0.078, which were measured for a practical cw pumped dye laser system by placing an acousto-optic modulator (EOM) inside the cavity. We used δ_S =0.004, R_s =0.001 to calculate and analyze the dependence of the absorption power of the sample on the optical density for the different numbers N of passes, and the results are shown in Fig. 3.10.

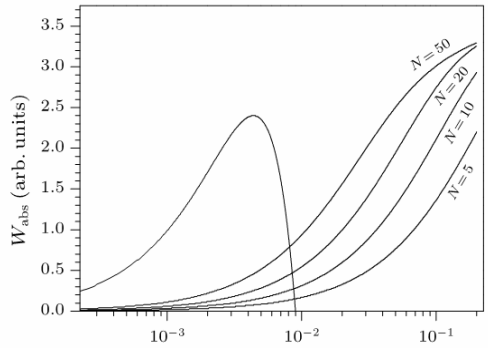

Fig. 3.10. Absorption power of the sample in the external cavity scheme with different numbers N of passes and the intra-cavity scheme as a function of the optical density. (Figure from ref. [19])

From Fig.3.10, we can find that for the low optical density, specially as $\alpha d < 0.008$, the absorption power in the intra-cavity scheme is far high than that in the extra-cavity one. However, when $\alpha d > 0.01$, because the losses from the sample approach the laser threshold, the absorption power will be sharply decreased. So in the region of the large optical density, the absorption power in the extra-cavity scheme is far higher than one in the intra-cavity one. As shown in Fig. 3.10, if we increase the pass number N of the pump beam, the absorption power in the extra-cavity scheme will increase to even exceed one in the intra-cavity scheme.

4. Experiment studies on laser cooling of solids using cavity-enhanced technologies

In the above section, we discuss and compare the enhancement effect of laser cooling of solids in the multi-pass pump, intra-cavity and resonant extra-cavity schemes in some detail. In this section, we will review experimental researches on laser cooling of solids using the above cavity-enhanced schemes and its recent progress.

As early as 2003 years, Hoyt et al. at University of New Mexico[4] and LANL group did detailed experimental research on laser cooling of solids [8] by using the multi-pass scheme after proposing how to improve the absorption power of the pump laser. At the same year, Heeg proposed the two methods using the intra-cavity and extra-cavity scheme to enhance the absorption power for laser cooling of solids and comparing laser cooling efficiencies between the intra-cavity and extra-cavity schemes. Afterwards, Heeg' group demonstrates the intra-cavity solid-state laser cooling of solids in experiment[3]. Seletskiy's group and LANL did a series of experimental researches on the cavity-enhanced resonant absorption for laser cooling of solids and obtained some important progress. More recently, they have successfully completed a milestone work and realized laser cooling of doped-Yb^{+3} YLF crystal materials with a cryogenic temperature.

4.1 Cooling of Yb: ZBLAN using intra-cavity enhanced absorption

When a diode laser is used to pump a solid laser, the laser radiation will be oscillated in an optical resonant cavity, at the same time the intensity of laser in the cavity will be amplified due to the simulation emission of laser gain medium. After the intensity of laser in the optical resonant cavity exceeds its threshold, the laser will be output from the cavity[26]. If inserting a solid sample with a low loss into the optical cavity, but the excited wavelength can be sustained to be oscillated in the cavity, and then the intra-cavity enhanced laser will increase the resonant absorption of the sample, which will result in an efficient laser cooling for solids in the laser cavity. As discussed in section 3.1, the almost materials used to form optical refrigeration has a low optical density (i.e., a low absorption), so one can use this intra-cavity enhanced scheme to realize laser cooling of solids. By choosing some optimal parameters, the intra-cavity enhancement scheme will become an efficient laser cooling method. In 2004, Heeg' group demonstrated the intra-cavity solid-state laser cooling scheme for solids experimentally [3] and the corresponding experiment setup is shown Fig. 4.1. In their experiment, the $Yb^{3+}KY(WO_4)_2$ (KYW) gain medium (10% doped, 1mm length, antireflection coated) was pumped along its b axis in the longitudinal direction by either one or two counter-propagating diode laser ($1\times100\mu m$) at 981.2nm. The diode laser was focused into the gain medium, which was

placed at the confocal center of a Z cavity, by using two concave mirrors with a high reflectivity at 1020-1060nm and a high transmission at 981.2nm. About 3W laser power per diode was illuminated on the gain medium due to the reflection losses from the pump optics. A Brewster prism was used to tune the excited wavelength from about 1020nm to 1040nm. A spatial filter was utilized here to minimize the residual radiation and super fluorescence on the cooling medium. An output coupling mirror with a 2% transmission was used to output a laser beam with the maximum power of up to 800mw at 1032nm when the power each diode laser is 1.2W. The intracavity circulating powers was be increased to 180W by using a high reflectivity mirror.

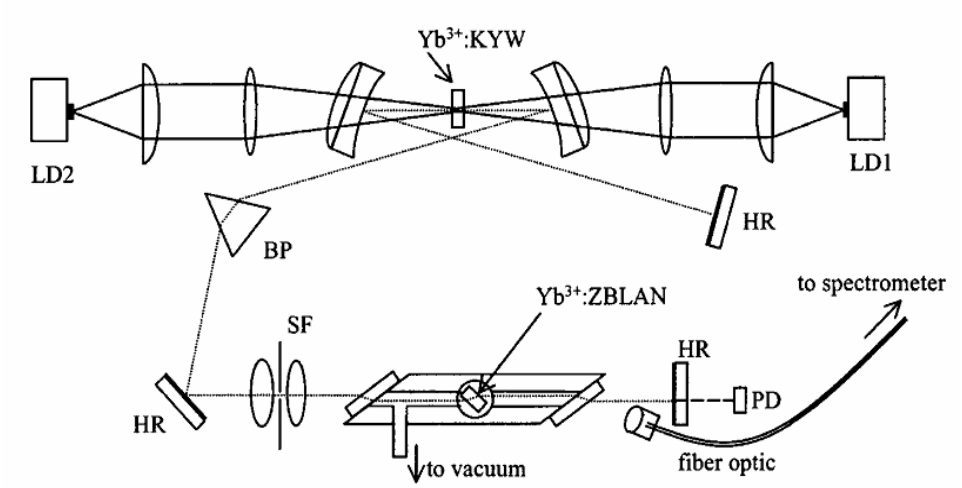

Fig. 4.1. Schematic of intra-cavity enhancement laser cooling of solids. LD is the laser diode, PD is the photodiode, HR is the high reflector, BP is the Brewster tuning system, and SF is the spatial filter. (Figure from ref. [3])

The cooling medium, a 2% doped Yb^{3+}: ZBLAN rectangular glass with dimensions $2 \times 2 \times 3$ mm, is used in this experiment, and the end-faces of the cooling medium is cut as a Brewster's angle in order to reduce the reflection losses of the sample surfaces. In the experiment, the temperature change of the sample is measured by a noncontact fashion according to the fluorescent spectral narrowing with decreased homogeneous broadening at lower temperatures. They measured the temperature drop spectrum of the cooling sample with a 2mm length, and the results are shown in Fig. 4.2.

In this experiment, the gain medium was pumped by two diode laser and the pump power in the cavity was up to 125W. After 10 minutes the sample reached the new thermal equilibrium and its temperature dropped to 6 K from the ambient temperature. At the same time, the heat sink's temperature rises by 3K due to absorbing the scatter laser and fluorescent emitted by the sample.

This experiment demonstrated the intra-cavity enhancement for laser cooling of solids. Because the absorption of cooling medium is low and the laser power for the optical refrigerator is not very high, so this approach is a prospect method for future optical refrigerator. The temperature drop of the cooling medium is not large in this experiment

due to not enough pure of the sample and resulting in parasitic heating[27], the thermal radiation from the chamber, the conductive thermal from the supporter, the reapportion fluorescent[28, 29, 30], however, these problems will be improved in the future along with the advance of material fabrication[9], low emissivity coating and so on. Furthermore, introducing the Brewster prism to tune the wavelength is very important for cooling the sample to the cryogenic temperature. This is because with the temperature drop the population in the ground upper multi-levels will be decreased, so it must adjust the wavelength to the short wavelength so as to weaken the decreasing absorption of the pump beam, and is able to obtain the cryogenic temperature[11,31]. Finally, the intra-cavity cooling approach has prosperously perspective for the practical optical refrigerator.

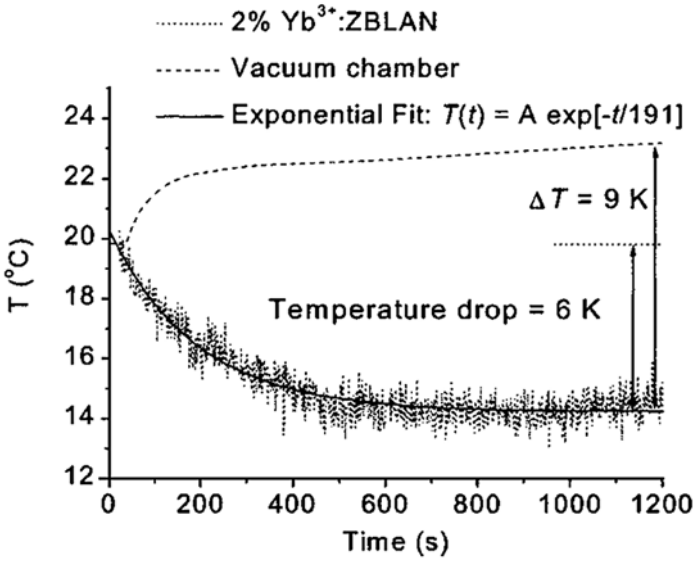

Fig. 4.2. The temperature change of the sample with a 2mm length and the heat sink as function of time (Figure from ref. [3])

4.2 Cooling of Yb: ZBLAN using extra-cavity enhanced resonant absorption

The multi-pass scheme make great successful in laser cooling of solids in Ref [12] and obtain 143K temperature drop from room temperature, but it has own disadvantage. One of the fundamental defects is a hole on the end-face of the sample because it will introduce light scattering (parasitic loss) and leak the pump light. Another shortcoming is the mirror deposited on another end-face of the sample, which will lead to the parasitic heating. The intra-cavity scheme has some advantages, such as the higher pump laser intensity in the cavity and an adjustable pump wavelength by the Brewster tuning prism[3], but it has not been adopted usually due to more optical components in the cavity and the complexity of operation. So it goes against to develop a practical optical refrigeration due to these disadvantage of the above two schemes. Fortunately, the extra-cavity resonant enhancement laser cooling scheme for solids offers a relatively simple and feasible technology for optical refrigeration.

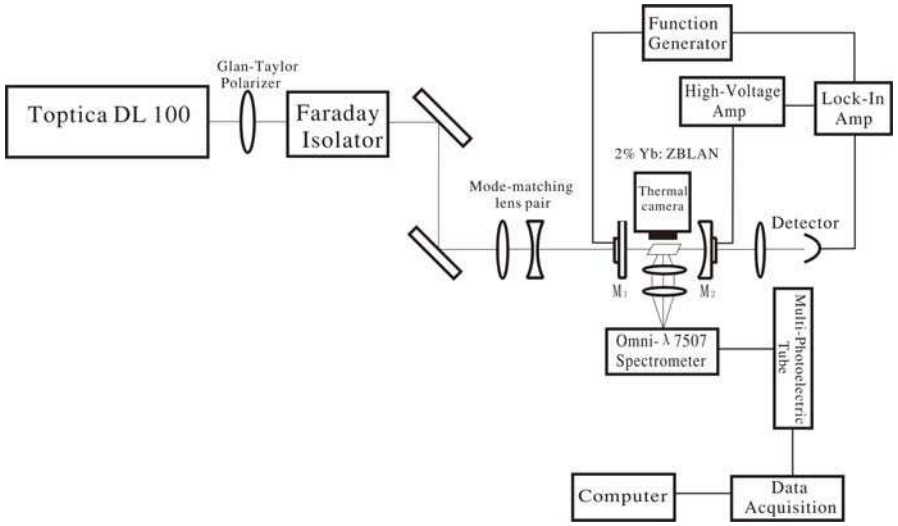

Fig. 4.3. Schematic experimental setup of the extra-cavity resonant enhancement laser cooling

The schematic experimental setup for extra-cavity enhancement resonant absorption for laser cooling of solids is shown in Fig. 4.3. The cavity is made up of two mirrors, and the first mirror M_1 is the input coupling mirror with a reflectivity of 95%, which can be adjusted to the proper value so as to obtain the maximum resonant absorption of cooling medium according to the absorption of the cooling material and the loss in the cavity. The reflectivity of the second mirror M_2 is almost equal to unity. In this experiment, the laser wavelength should be resonant with the optical cavity with a length of l so that one can obtain the maximum power in the cavity and the maximum absorption of cooling medium. A small amplitude signal generated by the function generator is used to dither the cavity, and then the intensity of laser is modulated, simultaneously, this signal is also input into Lock-In Amplifier as a reference signal. The dithered transmission is monitored by the photo-detector and mixed it with the reference signal from the function generator in Lock-In Amplifier. Then the error signal demodulated by Lock-In Amplifier was feedback to the PZT on the mirror after amplified by the High-Voltage Amplifier. Thus one can keep the laser frequency to be resonant with the frequency of cavity. The temperature of solid sample can be monitored by the thermal camera or Differential luminescence thermometry[32-35]. In 2006, D. Seletskiy et al studied the cavity enhanced resonant absorption for laser cooling of Yb^{3+} ZBLAN glass in experiment[13]. A commercial laser (ELS, VeraDisk Yb: YAG) with the maximum output power of about 45W at 1030nm was used. To avoid the laser unstable due to the optical feedback, a Faraday isolator (EOT, Model# 4I1030) with > 30dB isolation was used. The MML_2 and MML_1 (MML_1 with f1=50 mm, MML_2 with f2=100mm) coating with anti-reflection coat for 1030nm on their sides was used to enable the laser beam has a proper divergence and a proper transverse mode inside the cavity[26]. The input–coupler was mounted on the 3-axis piezo-controllers (Thorlabs, Part#MDT693) to control the transverse mode of the cavity to match with that of the laser. The reflectivity of the coating on the sample end-face serve as high reflection mirror is higher than 99.9%.

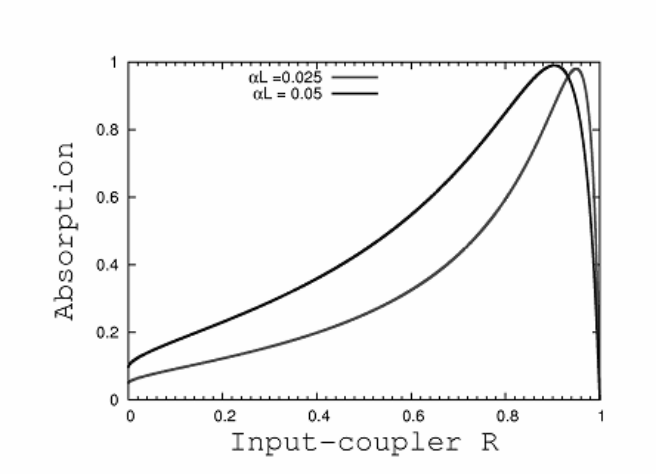

Fig. 4.4. The relationship between the cavity-enhanced absorption and the input-coupler reflectivity for two different values of αl (Figure from ref. [13])

From the extra-cavity enhancement theory in section 3.1, D. Seletskiy calculated the input-coupler reflectivity as a function of the sample absorption for different optical density αl, and the results are shown in Fig. 4.4. In the experiment, D. Seletskiy et al demonstrated the absorption enhancement for two different input-coupler reflectivities, and the results are shown in Fig. 4.5. We can see from the theoretical calculation (see Fig.4.4) and the experimental results (see Fig.4.5) that the experimental data are in good agreement with the theoretical results, which can be further found in Fig. 4.6. In this work, D. Seletskiy et.al did not give the temperature drop of the sample, but just to prove the enhancement of resonant absorption of Yb: ZBLAN glass sample by a factor of 11 compared to the double-pass configuration. This is the great significance meaningful work because it has relatively simple optical arrangement and great enhancement of the absorption for the cooling sample.

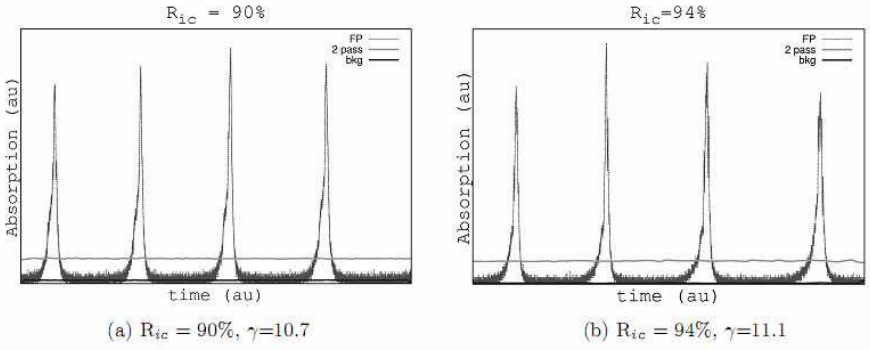

Fig. 4.5. Experimental demonstration of the absorption enhancement for two different input-coupler reflectivities $R_{ic} = 90\%$ and 94%, respectively (Figure from ref. [13])

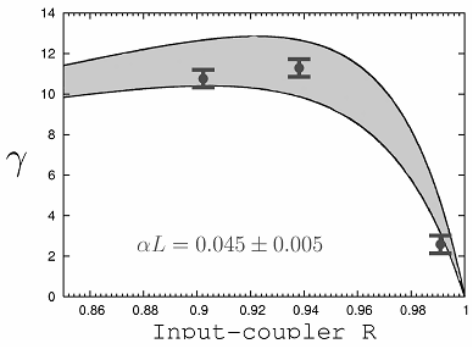

Fig. 4.6. The dependence of the enhancement absorption factor on the reflectivity of Input-coupler, and the shaded region represents uncertainty in the measured value of $\alpha l=0.0045 \pm 0.005$. The enhancement factors γ are plotted in the same scale, which is obtained from the experiments with different reflectivities (90%, 94%, 99%) and show very good agreement with the expected values, calculated from Eq 3.14. (Figure from ref. [13])

After this work, D. Seletskiy et al did a series of work to improve the extra-cavity enhancement for laser cooling of solids and made the great achievements, and nearly 20 fold of enhancement of the resonant absorption are obtained.

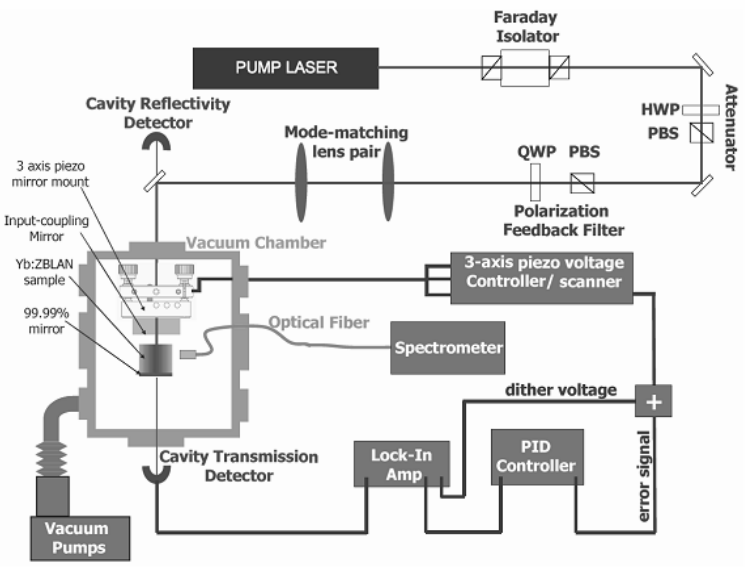

Fig. 4.7. Experimental setup of extra-cavity resonant enhancement scheme for laser cooling of solids. The thin lines are the optical beam path, and the thicker lines are electronic connections. (Figure from ref. [10])

Fig. 4.7 is the improved experimental setup. In this experiment, the reflectivity of the dielectric mirror is greater than 99.99%, and the sample was supported by 4 quartz 600μm

diameter fiber. The sample was placed in a clam-shell, which was placed in the aluminum vacuum chamber with 8 vacuum ports, and the windows were coated by AR coating to increase the transmission of the pump laser. The inside surfaces of clam-shell chamber are painted with a preferential low-emissivity Maxorb coating, which is a gold-plated copper. The cavity is kept on working resonant with the pump wavelength and is stabilized via an electronic feedback loop.

In this experiment, they obtained the absorption efficiency up to $91 \pm 2\%$, and the temperature drop was about 3K, which was measured by a noncontact method, so-called differential luminescence. This measurement method is so sensitive that can resolve a 0.1K temperature change by resolving the temperature change from the reference spectra.

In 2008, D. Seletskiy et al studied the cavity resonant-enhanced laser cooling of Yb^{3+}: YLF crystal and obtained the temperature drop of about 70 degrees from the ambient temperature. In the experiment, the sample was cut with a Brewster angle to reduce the Fresnel loss in the end-faces of the sample, and the cavity is also formed in Brewster geometry for the p-polarized pump light. Fig. 4.8 is the photograph of Brewster geometry cavity. From Fig.4.8, we can see that in order to reduce the loss of cavity, the mirrors should be almost contacted with the sample.

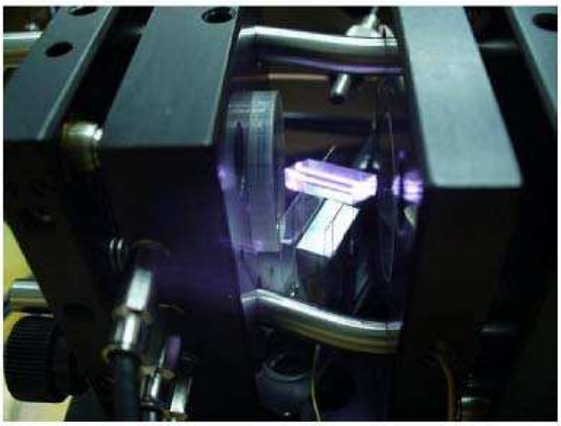

Fig. 4.8. Photograph of the Brewster geometry cavity. The left mirror of the image is the input coupler mounted on the 3-axis piezo mirror mount. The fiber above the sample is used for collecting luminescence. False color luminescence is visible in the sample, induced by pump light trapped on resonance. (Figure from ref. [17])

Fig. 4.9 shows the experiment results on the temperature drop of the sample for the different input power. Due to the sample so close to the mirror, the fluorescent emitted from the sample will be absorbed by the mirror. Simultaneously, the mirror with a nearly unity emissivity at the thermal wavelengths radiates on the sample and heats it. So the temperature drops of the Yb: YLF crystal is up to 69K from the room temperature. This is the cooling record for crystalline solids, but it not achieves the minimum achievable temperature (MAT). However, under the ideal conditions, the MAT could be achieved to $170 \pm 10K$ [12].

In this year, D. V. Seletskiy investigate the resonant cavity-enhanced absorption for optical refrigeration with a low-power laser and find the 20-fold increase over the single path absorption with the low loss medium (Yb^{3+}-doped ZBLAN glass[23]) placed in the resonant

cavity mentioned. Their experiment setup is shown in Fig. 4.10. The 2% Yb^{3+}-doped ZBLAN glass was placed in the cavity, and one end-face of the sample was coated as a high reflectivity of mirror (R>0.999), and another face of the sample was deposited a anti-reflection coating to decrease Fresnel loss on the surface.

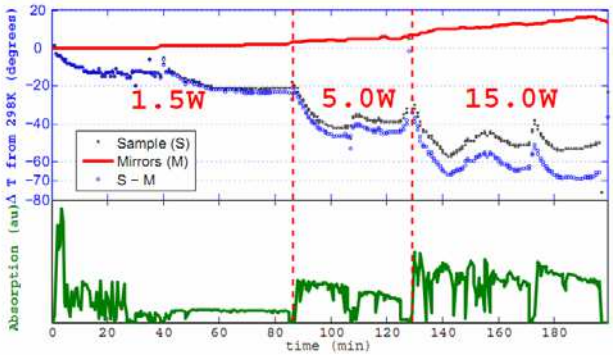

Fig. 4.9. The top graph shows the temperature dynamics Δ T(offset to zero at 298K). The grey closed circles, the red solid line and the blue open circles represent the temperature change of the sample, cavity mirrors and the difference temperature of the chamber and sample, respectively. The bottom graph is the absorption on linear scale in arbitrary units. (Figure from ref. [17])

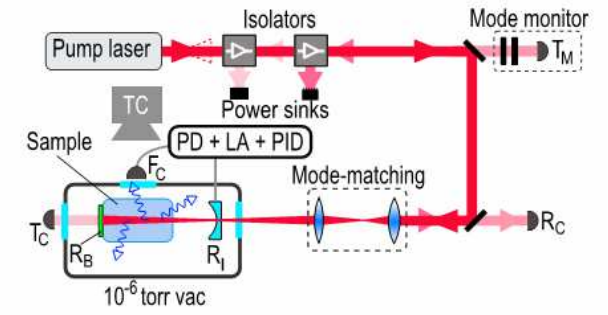

Fig. 4.10. The arrangement of experimental setup. PD+LA+PID is the proportional -integral-derivative circuit, PD is the piezo driving circuit, LA is the lock-in amplifier, which are used to control the cavity length to keep stabilization. TC is the thermal camera for monitoring the cooling process. (Figure from ref. [23])

To optimize the maximum pump laser coupled into the cavity, the reflectivity of the input mirror is usually equal to the value of $R_{ic} = e^{-\alpha l}$. The input mirror with a reflectivity of R=94% is housed in a piezo-actuated mount, allowing for cavity length scanning and stabilization. Moreover, to minimum the heat load adding to the sample, thin quartz fibers used to support the sample, which is placed in a tightly fitted shell with a low-emissivity coating. The cooling process is recorded by the thermal camera. Due to the transmission and losses are minimized by design, so the absorption A can be deduced from A=1-R_c. In the Gires-Tournois limit, the pump absorption at resonance can be expressed as[23]

$$A = 1 - \left(\frac{\sqrt{R_I} - e^{-\alpha l}}{1 - e^{-\alpha l}\sqrt{R_I}}\right). \tag{4.1}$$

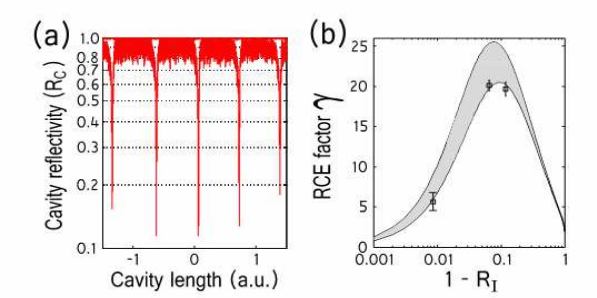

Fig. 4.11. (a) Resonant 89% absorption of the cavity plotted on a semi-log scale. (b) The experiment data agree with model fitting results, according to Eq. 4.1. (Figure from ref. [23])

Fig. 4.11 (a) shows the relationship between the cavity reflectivity and the cavity length. From Fig.4.11(a), we can find that the maximum absorption reaches to $89 \pm 3\%$ when the cavity length are scanned. From Fig. 4.11 (b), it is clear that the resonant cavity enhancement factor is up to 20 fold compare with single-time passing the sample. Fig. 4.10 is the experimental results of cooling process and the temperature drop of the sample. To avoid the saturation of the thermal camera image, the sample was radiated by the pump laser with a 1W power for 40 minute.

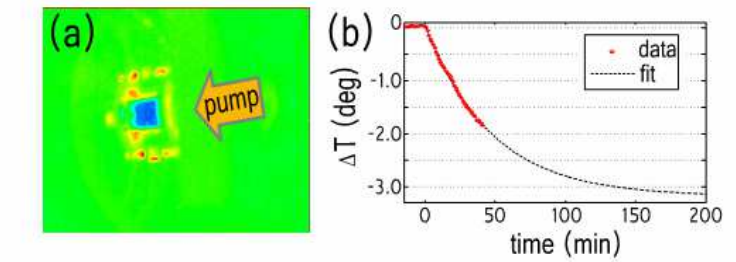

Fig. 4.12. (a) Top view thermal image of the cavity at resonance. Blue area represents the sample, the green area represents the ambient and light gray structure around the sample is the shell, which is heat by the fluorescence absorption. (b) The red line is the experiment measurement data, and the gray dot line is the fitting one. (Figure from ref. [23])

By fitting the experimental data to $\Delta T(t) = \Delta T_f[1 - \exp(-t/\tau)]$, they obtain the final temperature drop of $T_f = -3.2 \pm 0.1K$ from the ambient. Form the fitting formula, the thermal time constant is $\tau = 45$ min. In the case of small input power, the temperature drop linearly scales to be imperfect efficiencies. The ratio of absorption, stabilization, radiation shielding are 90%, 60%, and 30% respectively. It can be estimated that the final temperature drop is $3.2 \times [0.9 \times 0.6 \times 0.3]^{-1} = 20K/W$. The difference between the above mentioned final temperature drop per unity power of incident laser (20K/W) and the best cooling performance of $\sim 22K/W$ in Yb: ZBLAN glass can be ascribed to the variation of the impurity of the different sample.

5. Conclusions and outlook

In this chapter, we have reviewed various enhancement means of the pump beam to facilitate laser cooling of solids, and especially discussed the multi-pass pump, extra-cavity and intra-cavity resonant enhancement absorption in some detail from their principles to the experiment technologies. Although the multi-pass pump scheme has a lower absorption enhancement relative to two other schemes, it has simple operation and less optical elements. Therefore one hope to find some more efficient material for laser cooling or develop some high purity of solids, and first using the multi-pass pump scheme to do experimental researches on laser cooling of solids, such as using Yb^{3+} -doped ZBLAN and Yb^{3+} -doped YLF materials in the experiments. So the multi-pass scheme can compete with other two cavity-enhanced ones in the factual optical refrigerator. The intra-cavity enhancement scheme can greatly enhance the intensity of the pump laser in the cavity when the low-loss cavity and low absorption of cooling medium is used, however, due to the complication of technology and more optical elements, it will lead to some obstacles for forming a feasible optical refrigerator. In particular, it will be no suitable for some cooling materials with a large absorption. Since the extra-cavity enhancement scheme is a relatively simple technology and has a large enhancement of resonant absorption, it would be chosen as one of the practical or useful optical refrigerators.

The scientists have used the three different schemes mentioned above to investigate laser cooling of solids in experiment and hoped to find a more feasible technology for the future optical refrigeration. By optimizing the experiment parameters, one hope to obtain the maximum temperature drops of laser cooling samples. Furthermore, by probing some new coating materials to shield the thermal radiation more effectively, adjusting the geometry of the sample, and reducing the impurity of the sample, one hope to find some new paths to a practical optical refrigerator. Recently, D. V. Seletskiy utilizing the extra-cavity resonant enhancement scheme to improve the pump laser absorption by up to 20 folds compared with the single pass pump one. In this year, especially, laser cooling of solids to cryogenic temperatures using the multi-pass enhancement absorption shows a new dawn to develop a promising optical refrigerator. Since such an all-optical refrigerator has some novel and unique advantages, such as a mini volume, lightly weight, electromagnetic radiation free, non-vibration, non-noise, and long lifetime, etc, it will become an irreplaceable cryogenics in the fields of military, space technology, integrated optics, micro-electronics, remote sensing and telemetering, and so on.

6. Acknowledgments

We acknowledge the support from the National Natural Science Foundation of China under Grant No. 10974055.

7. References

[1] R. I. Epstein, M. I. Buchwald, B. C. Edwards, T. R. Gosnell. C. E. Mungan, *Nature*, 1995, Vol. 377(12): 500-502.

[2] B. Heeg, G. Rumbles, A. Khizhnyak, P. A. DeBarber, *J. Appl. Phys*, 2002, Vol. 91(5): 3356-3362

[3] B. Heeg, M. D. Stone, A. Khizhnyak, G. Rumbles, G. Mills, P. A. DeBarber, *Phys. Rev*. A, 2004, Vol. 70: 021401(1-4)

[4] Chad. William. Hoyt, The University of New Mexico, PHD May 2003

[5] C. W. Hoyt, M. Sheik-Bahae, R. I. Epstein, B. C. Edwards, and J. E. Anderson, P*hys. Rev. Lett*, 2000, Vol. 85 (17): 3600-3603
[6] T. R. Gosnell, *Opt. Lett*. 1999, Vol. 24: 1041-1043
[7] X. Luo, M. D. Eisaman, and T. R. Gosnell, *Opt. Lett*. 1998, Vol. 23: 639-641
[8] C. W. Hoyt, M. P. Hasselbeck, M. Sheik-Bahae, *J. Opt. Soc. Am.* B, 2003, Vol. 20, (5) 1066-1074
[9] M. P. Hehlen, R. I. Epstein, *SPIE, 2007*, Vol. 6461, 646103(1-6)
[10] W. M. Pattersona, M. P. Hehlenb, M. Sheik-Bahaea, R. I. Epstein, *SPIE*, Vol. 7228: 72280C(1-10)
[11] R. I. Epstein, M. Sheik-Bahae, Optical Refrigeration science and applications of laser cooling of solids, 2010
[12] D. V. Seletskiy, S. D. Melgaard, S. Bigotta, A. D. Lieto, M. Tonelli, M. Sheik-Bahae, *Nature Photonics*, 2010, 17: 161-164
[13] D. Seletskiy, M. P. Hasselbeck, M. Sheik-Bahae, J. Thiede, R. I. Epstein, *SPIE 2006*, Vol 6130: 61300p(1-8)
[14] Y. H. Jia, B. Zhong, J. P. Yin, Chin. *Phys. Lett*, 2008, Vol. 25(1): 85-88
[15] D. Seletskiy, M. P. Hasselbeck, M. Sheik-Bahae, R. I. Epstein, *SPIE, 2007*, Vol. 6461: 646104(1-8)
[16] Y. H. Jia, B. Zhong, J. P. Yin, *Chin. Opt. Lett*, 2008, Vol. 6(11): 848-851
[17] D. Seletskiy, M. P. Hasselbeck, M. Sheik-Bahae, R. I. Epstein, S. Bigottac, M. Tonelli. *SPIE 2008*, Vol. 6907: 69070B(1-9)
[18] D. V. Seletskiy, S. D. Melgaard, M. P. Hasselbeck, M. Sheik-Bahae, R. I. Epstein, S. Bigottac, M. Tonelli, *SPIE, 2009*, Vol. 7228: 72280F(1-4)
[19] Y. H. Jia, B. Zhong, J. P. Yin, *Chin. Phys. Lett*, 2010, Vol 7: 073201(1-4)
[20] M. Born, E. Wolf, *Principled of Optics* (Seventh Edition)
[21] A. Rayner, N. R. Heckenberg, H. Rubisztein-dunlop, *J. Opt. Soc. Am*. B, 2003, Vol. 20(5): 1037-1052
[22] L. H. Kou, D. Labrie, P. Chylek, *Applied. Optics* 1993, Vol. 32(19): 3531-3540
[23] D. V. Seletskiy, M. P. Hasselbeck, M. Sheik-Bahae, *App. Phy. Lett,* 2010, Vol. 96: 181106(1-4)
[24] C. E. Mungan, M. I. Buchwald, B. C. Edwards, R. I. Epstein and T. R. Gosnell, *Phys. Rev. Lett,* 1997, Vol. 78(6), 1030-1033
[25] G. Labeyrie, A. Landragin, J. V. Zanthier, R. Kaiser, N. Vansteenkiste, C. Westbrook. A. Aspect, *Quantum. Semiclass. Opt*, 1996, Vol. 8: 603–627.
[26] A. E. Siegman, Lasers, University Science Books, Sausalito, 1986
[27] J. C. Fajardo,G. H. Sigel Jr, B. C. Edwards, R. I. Epstein, T. R. Gosnell, C. E. Mungan, *J. Non-Cryst. Solids*, 1997, Vol. 213&214: 95-100
[28] B. Heeg, G. Rumbles, *J. Appl. Phys.* 2003, Vol. 93(4): 1966-1973
[29] B. Heeg, P. A. DeBarber, and Garry Rumbles, *Applied. Optics*, 2005, Vol. 44(15): 3117-3124
[30] X. F. Wang, S. L. Chang, J. K. Yang, M. Zhou, D. X. Cao, J. C. Tan, *Applied. Optics*, 2007, Vol. 46(35): 8446-84452
[31] M. Sheik-Bahae, R. I. Epstein, Nature. *Photonics*, 2007, Vol. 1: 693-699
[32] B. Imangholi, M. P. Hasselbeck, D. A. Bender, C. G. Wang, M. Sheik-Bahae, R. I. Epstein, S. Kurtz, *SPIE, 2006*, Vol. 6115: 61151C(1-6)
[33] W. Patterson, E. Soto, M. Fleharty, M. Sheik-Bahae, *SPIE, 2007*, Vol. 6461: 64610B(1-6)
[34] D. V. Seletskiy, M. P. Hasselbeck, M. Sheik-Bahae, R. I. Epstein, *SPIE, 2009*, Vol. 7228: 72280K(1-5)
[35] W. M. Patterson, D. V. Seletskiy, M. Sheik-Bahae, R. I. Epstein, M. P. Hehlen, 2010, *J. Opt. Soc. Am.* B, Vol. 27 (3): 611-618

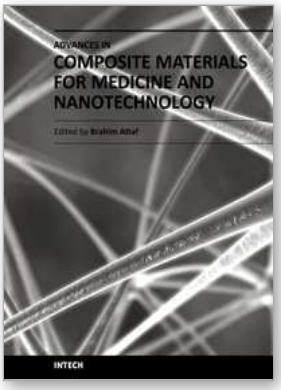

Advances in Composite Materials for Medicine and Nanotechnology

Edited by Dr. Brahim Attaf

ISBN 978-953-307-235-7
Hard cover, 648 pages
Publisher InTech
Published online 01, April, 2011
Published in print edition April, 2011

Due to their good mechanical characteristics in terms of stiffness and strength coupled with mass-saving advantage and other attractive physico-chemical properties, composite materials are successfully used in medicine and nanotechnology fields. To this end, the chapters composing the book have been divided into the following sections: medicine, dental and pharmaceutical applications; nanocomposites for energy efficiency; characterization and fabrication, all of which provide an invaluable overview of this fascinating subject area. The book presents, in addition, some studies carried out in orthopedic and stomatological applications and others aiming to design and produce new devices using the latest advances in nanotechnology. This wide variety of theoretical, numerical and experimental results can help specialists involved in these disciplines to enhance competitiveness and innovation.

INTECH
open science | open minds

InTech Europe
University Campus STeP Ri
Slavka Krautzeka 83/A
51000 Rijeka, Croatia
Phone: +385 (51) 770 447
Fax: +385 (51) 686 166
www.intechopen.com

InTech China
Unit 405, Office Block, Hotel Equatorial Shanghai
No.65, Yan An Road (West), Shanghai, 200040, China
中国上海市延安西路65号上海国际贵都大饭店办公楼405单元
Phone: +86-21-62489820
Fax: +86-21-62489821